

Hydrazine Decomposition over Ir_n/Al₂O₃ Model Catalysts Prepared by Size-Selected Cluster Deposition

Sungsik Lee, Chaoyang Fan, Tianpin Wu, and Scott L. Anderson*

Department of Chemistry, University of Utah, Salt Lake City, Utah 84112

Received: August 30, 2004; In Final Form: October 13, 2004

Hydrazine decomposition chemistry was probed over a temperature range from 100 to 800 K for a series of model catalysts prepared by mass-selected Ir_n⁺ deposition on planar Al₂O₃/NiAl(110). Two sets of experiments are reported. Temperature-programmed desorption (TPD) was used to study hydrazine desorption and decomposition on Al₂O₃/NiAl(110) and on a model catalyst prepared by deposition of Ir⁺ on Al₂O₃/NiAl(110) at a density large enough ($5 \times 10^{14} \text{ cm}^{-2}$) that formation of a distribution of small Ir_n clusters on the surface is expected. This model catalyst was found to have hydrazine decomposition properties qualitatively similar to those observed on single-crystal Ir and polycrystalline Rh. This catalyst was also studied by X-ray photoelectron spectroscopy (XPS), to probe TPD-induced changes in the samples. A substantial decrease in the Ir XPS intensity suggests that considerable sintering takes place when the samples are heated to 800 K. In addition, a significant fraction of the nitrogen contained in the hydrazine is converted to an aluminum nitride (or mixed Al_xO_yN_z) compound. Continuous flow experiments were used to probe relative reactivity at 300 and 400 K of samples prepared by depositing differently sized Ir_n⁺ clusters. At 300 K, samples prepared with preformed Ir_n⁺ ($n = 5, 7, 10$) are about twice as active, per Ir atom, as samples prepared with Ir⁺ deposition, and there is a weaker trend to higher activity with increasing cluster size. At 400 K the trends are similar, but weaker, suggesting that thermal modification of the samples is already significant.

I. Introduction

Decomposition of hydrazine and ammonia on metal surfaces^{1–8} and supported metal particles^{9,10} is important for the fundamental understanding of several industrial catalytic processes, including monopropellant thrusters, gas generators, and pure hydrogen production for electric fuel cells.¹¹ The standard commercial catalyst used for thrusters and gas generators is iridium on Al₂O₃ (e.g., Shell 405), chosen because it combines reasonable activity and high thermal stability. There are several problems with deactivation of such catalysts in long exposures to hydrazine. High-temperature reaction conditions may induce sintering of the small metal particles, and strongly bound nitrogen species left on the catalyst surface may poison the catalyst. For applications with intermittent operation, there is the additional problem of cold starts. If the catalyst is not active enough at low temperatures, then liquid hydrazine can fill the catalyst pores, and when decomposition finally takes off, the resulting high pressures can fragment the support material. The ideal catalyst for thruster applications should combine high activity down to cryogenic temperatures with long-term stability at high reaction temperatures.

The metal in such a catalyst is present as a distribution of nanoparticles on the alumina surface. Ir particle size effects have been explored by Gates and co-workers, using catalysts prepared by impregnation with organometallic iridium cluster compounds.^{12–14} For example, they showed substantial increases in activity for toluene hydrogenation as particle size increased from Ir₄ into the range of a few nanometers. To our knowledge there has been no systematic investigation of size effects on hydrazine chemistry on small supported Ir clusters.

Here we report a study of hydrazine decomposition on planar model catalysts prepared by Ir_n⁺ deposition on planar Al₂O₃ films in an ultrahigh vacuum (UHV). A combination of mass spectrometry and electron spectroscopic analysis was used to probe hydrazine decomposition and the resulting changes in sample electronic structure and surface composition. Two related studies are presented. To approximate the behavior of a conventional supported catalyst, samples were prepared by depositing relatively high coverages of Ir atoms on the surface, with the expectation that agglomeration should result in a distribution of small Ir clusters. Chemistry on this model catalyst was studied over a wide temperature range, and X-ray photoelectron spectroscopy (XPS) was used to probe sintering and formation of surface nitrogen compounds. In addition to providing a point of comparison for the size-selected cluster work, these experiments are useful because they are the first hydrazine/Ir/Al₂O₃ studies extending to cryogenic temperatures, where Ir single-crystal work has found interesting chemistry. The second set of studies were for model catalysts prepared by low-coverage deposition of size-selected Ir_n⁺, allowing us to examine the effects of Ir cluster size on the reactivity.

It would be nice to compare our results for Ir_n/Al₂O₃/NiAl with results for high-surface-area catalysts. The only detailed work on hydrazine/Ir/Al₂O₃ high-surface-area catalysts is that of Falconer and Wise.⁹ They studied temperature-programmed desorption (TPD) and also reactions under steady flow conditions, but there are enough differences in the experiments to make direct comparisons difficult. Their experiments were all above room temperature and at atmospheric pressure, where the steady-state surface coverages are much higher than in our experiments. In addition, their catalyst (Shell 405) also had quite high Ir coverage—reported as 32 wt % Ir on low-surface-area

* To whom correspondence should be addressed. E-mail: anderson@chem.utah.edu.

granular alumina. In TPD they observed ammonia desorbing at temperatures between 350 and 650 K, and H₂ desorbing between ~350 and 900 K, in both cases with clear bimodal temperature dependence. In addition, N₂ was observed to desorb between ~600 and 800 K. In steady flow reaction conditions, exclusively NH₃ product is observed for $T < 600$ K, and then the products rapidly switch to a mixture of N₂ and H₂. It is difficult to know how to compare these results with our results under UHV conditions. Fortunately, there are a number of UHV metal surface chemistry studies (see below) which are directly comparable. Therefore, in the Discussion, we interpret our results in light of the mechanisms deduced in these detailed UHV studies.

II. Experimental Section

The experiments were carried out in a vacuum system consisting of a previously described mass-selected ion deposition beamline,¹⁵ coupled to a new UHV end chamber with a base pressure $< 2 \times 10^{-10}$ Torr. The UHV chamber incorporates facilities for sample preparation, XPS, Auger electron spectroscopy (AES), and ion scattering spectroscopy (ISS). It also includes a differentially pumped mass spectrometer for temperature-programmed desorption/reaction (TPD/TPR) studies. The sample can be transferred and isolated in a second chamber that serves as a high-pressure cell and load-lock. While the end chambers are new, our operating and analysis procedures are similar to those previously described.^{16,17} The XPS experiments were carried out using a Mg K α (1253.6 eV) X-ray source, and binding energies were calibrated using the O and Al peaks of Al₂O₃, in turn calibrated against the Au spectrum of a gold foil. Sample temperatures were measured by a K-type thermocouple which was first spot-welded to a thin tantalum foil (0.005 mm thick) to prevent diffusion of nickel and aluminum between the thermocouple junction and the NiAl(110) crystal used as a substrate for Al₂O₃ growth. The protected thermocouple was then spot-welded to the back of the NiAl(110) crystal. The sample can be resistively heated to 1300 K and cooled to 90 K.

The Al₂O₃ support was prepared by oxidizing single-crystal NiAl(110), using the method of Freund and co-workers.¹⁸ Their characterization by scanning tunneling microscopy (STM), low-energy electron diffraction (LEED), and ultraviolet photoelectron spectroscopy (UPS) showed that a well-ordered film results, with a structure similar to that of γ -Al₂O₃ (the typical catalyst support), and with a thickness (~5 Å) thin enough to perform electron spectroscopy without sample charging problems. A conductive support also allows us to set a well-defined deposition energy in our ion deposition experiments. The cluster ions are neutralized upon deposition by electrons from the support. The NiAl(110) single crystal (Surface Preparation Laboratory) was cleaned by repeated cycles of Ar⁺ bombardment followed by annealing at 1220 K. The cleanliness of the sample was frequently checked by XPS and ISS. After cleaning, 1200 langmuirs of O₂ was dosed at 550 K, and the resulting film was annealed at 950 K.¹⁹ Attenuation of the Ni 2p XPS signal intensity by the Al₂O₃ overlayer was used to estimate the film thickness, and the value (~5 Å) is in good agreement with the literature.¹⁸ Continuity of the Al₂O₃ film was verified by ISS, which showed no signal for exposed surface Ni atoms. The Al 2p XPS signal shows both metallic Al (binding energy ~73 eV) from the NiAl, and a shoulder at 75.2 eV from the Al³⁺, in agreement with the reported value.²⁰ Between each Ir_n⁺ deposition experiment, the film, together with all iridium and contaminants, was removed by 1 keV Ar⁺ sputtering, followed by annealing at 1000 K for 15 min and at 1220 K for 10 min, prior to growth of a new oxide film.

It was deposited onto freshly prepared Al₂O₃ films by mass-selected ion beam deposition. Ir_n⁺ was generated by laser vaporization of an Ir target inside a channel filled with ~3 atm of helium, and the nascent Ir-containing plasma was entrained and cooled by helium as it flowed down the ~5 cm channel, before expanding into the vacuum. Ions are collected by a quadrupole ion guide, where additional thermal collisions with residual helium (~10⁻¹–10⁻² mbar) may occur. The gas-phase cluster internal energy is not characterized, but is presumably near or below room temperature. This energy is not important because the final temperature is determined by the deposition substrate temperature, which can be varied as described above. More important is the translational energy distribution, which controls the distribution of impact energies. The translational distribution is measured by retarding potential analysis, and is less than 1 eV fwhm. The ion beam is bent 18° to facilitate separation from neutrals exiting the source, then guided into the UHV system, and mass-selected by three additional quadrupoles. Finally, the selected Ir_n⁺ beam is deposited onto the substrate at a controlled energy, with the spot size determined by a mask, and dosimetry by current measurement. Doses are reported in terms of fractions of a close-packed Ir monolayer (1 ML = 1.6 × 10¹⁵ atoms/cm²). For all studies reported here, the deposition energy was 1.0 eV/atom.

Hydrazine (98.5%) was purified with several freeze–thaw cycles using both liquid nitrogen and dry ice/acetone baths. Mass spectral analysis was performed and compared with standard hydrazine electron impact fragmentation patterns in the NIST mass spectral database.²¹ To study hydrazine decomposition, we used TPD with a linear heating rate controlled by a PID controller (Eurotherm 2404). Hydrazine was dosed from a variable leak valve. The mass spectrometer (UTI 100C) was differentially pumped, and biased at +150 V so that electrons from the ion source could not impact the sample, where they might induce decomposition of hydrazine.²²

One factor complicating the mass spectral analysis is that hydrazine undergoes electron-impact-induced fragmentation, generating substantial intensity at masses corresponding to the expected catalytic decomposition products N₂, NH₃, and H₂. In the results below, we have corrected the product spectra for this ionizer fragmentation as follows. In the hydrazine (mass 32) TPD spectrum there is a sharp low-temperature (158 K) peak attributed to desorption of multilayer hydrazine. Ionizer fragmentation of this hydrazine results in appearance of this same sharp peak in the spectra for N₂, NH₃, and H₂. Because the multilayer hydrazine desorbs intact, we can use the multilayer desorption peak as a built-in indicator of the contribution of hydrazine ionizer fragmentation to the product signal. To correct the N₂, NH₃, and H₂ spectra, we simply subtracted the hydrazine spectrum, first scaling it so as to just cancel the contribution from ionizer fragmentation of the multilayer hydrazine. For reasons discussed below, the subtraction process is not perfect; therefore, we emphasize that all peaks shown in the corrected spectra are also clearly visible in the raw data. For H₂, we show both subtracted and raw spectra to illustrate the correction process.

III. Results and Discussion

A. Hydrazine Adsorption and Decomposition on Ir/Al₂O₃. Figure 1 shows series of hydrazine (mass 32) TPD spectra as a function of exposure to hydrazine on a clean Al₂O₃/NiAl surface at 93 K (i.e., no Ir deposition). For clean Al₂O₃, only intact hydrazine desorbed, with no evidence for decomposition products. At low exposures (<0.2 langmuir), hydrazine desorbs

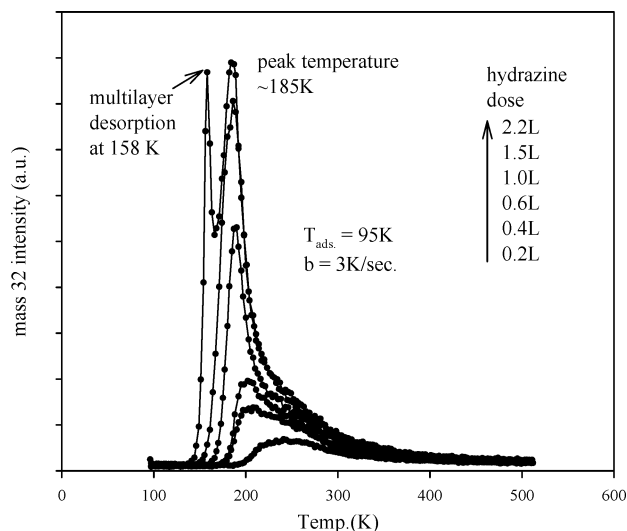


Figure 1. Temperature programmed desorption of hydrazine on Al₂O₃/NiAl(110) for several different initial doses of hydrazine, all at 93 K.

in a broad peak centered around ~ 245 K. With increased exposure, the peak narrows and shifts to lower temperature, resulting in a sharp peak at ~ 185 K for exposures of 1 langmuir and higher. This peak is attributed to hydrazine desorption from a nearly complete monolayer on the Al₂O₃/NiAl(110) surface. The broadening and shift to higher temperature at lower coverages represent either hydrazine desorbing from defect sites in the film or less repulsive lateral interactions at low coverage. For exposures over ~ 2 langmuirs, a new peak appears at 158 K, attributed to desorption from multilayer hydrazine (presumably mostly from a second layer on top of the more strongly bound first monolayer). The monolayer packing density of hydrazine on Al₂O₃/NiAl(110) is unknown, but can be estimated if we assume unit sticking probability for the 93 K hydrazine dose. From the absence of multilayer hydrazine at 1.5 langmuirs, and the relative intensities of the monolayer and multilayer peaks at 2.2 langmuirs, we estimate that the monolayer fills at a ~ 1.8 langmuir exposure, corresponding to $\sim 6.5 \times 10^{14}$ molecules/cm².

Figure 2 shows desorption spectra of hydrazine and its decomposition products, N₂, NH₃, and H₂, when Ir is present. The bottom frame shows raw TPD spectra for mass 32 (hydrazine) and mass 2 (H₂). The top frame shows spectra for H₂, NH₃ (mass 17), and N₂ (mass 28) that have been corrected, as discussed above, for contributions from ionizer fragmentation of hydrazine. The sample was prepared by deposition of 0.5 ML equivalent (8.0×10^{14} atoms/cm²) of Ir⁺ on Al₂O₃/NiAl(110). This density is high enough that some distribution of small Ir_n should form during deposition. This distribution probably changes during the course of a TPD experiment; therefore, each TPD run must use a freshly prepared sample. For this reason, we did not undertake a detailed study of the TPD dependence on hydrazine dose.

After Ir deposition, the samples were exposed to 2.7 langmuirs of hydrazine at 93 K, and then TPD was done at a 3 K/s heating rate. As on the clean alumina surface, a sharp desorption peak for hydrazine (mass 32, bottom frame, Figure 2) at 164 K is attributed to multilayer (i.e., mostly second-layer) desorption. The slightly higher temperature of this peak compared to that for clean Al₂O₃ (158 K) presumably reflects changes in the properties of the underlying monolayer hydrazine from interaction with the deposited Ir. As noted, the multilayer peak is used as an internal standard in correcting for ionizer fragmentation, hence the choice of a relatively high hydrazine exposure.

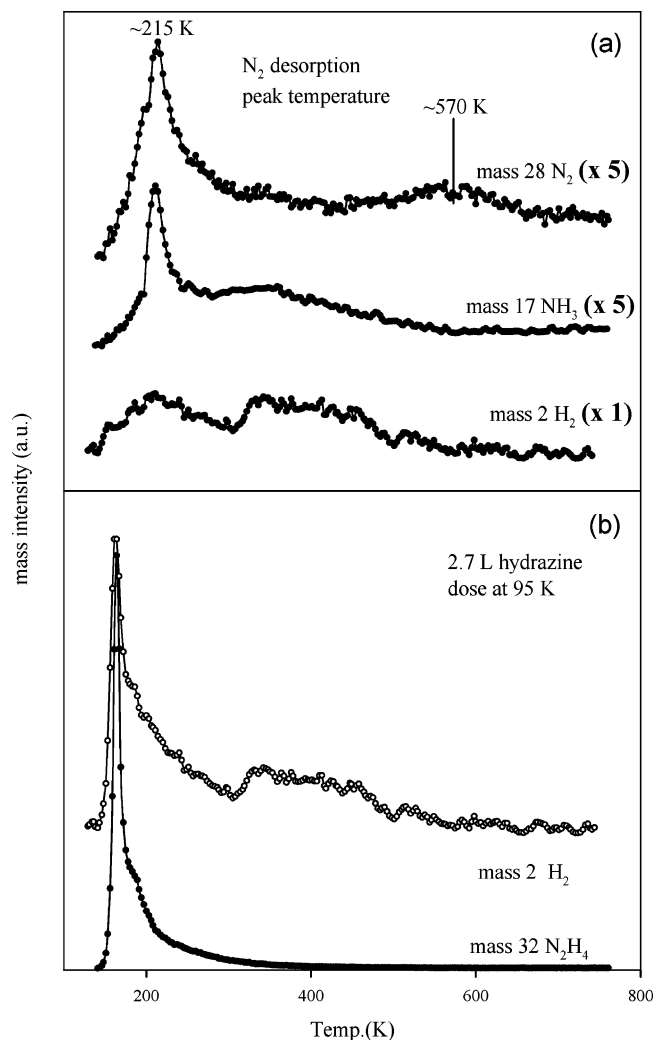


Figure 2. TPD spectra after 2.7 langmuir hydrazine exposure at 95 K, on a sample prepared by deposition of 0.5 ML of Ir⁺ on Al₂O₃/NiAl(110). Mass 28 is N₂, mass 17 is NH₃, mass 2 is H₂, and mass 32 is hydrazine. The heating rate was 3 K/s. Top frame: spectra for N₂, NH₃, and H₂, corrected for ionizer fragmentation of hydrazine. Bottom frame: spectrum of hydrazine, and raw spectrum for mass 2, showing the contribution from ionizer fragmentation of hydrazine.

One important question is whether the multilayer hydrazine desorbs intact or decomposes to some extent on Ir/Al₂O₃. If we assume that the first monolayer fills at a ~ 1.8 langmuir exposure, as on Al₂O₃, then comparison of the multilayer peak intensities for Al₂O₃ and Ir/Al₂O₃ (accounting for the different hydrazine doses) is consistent with intact desorption for most or all of the multilayer hydrazine.

Unlike clean alumina, there is no distinct peak corresponding to hydrazine desorption from the first monolayer. There is, however, a shoulder at ~ 185 K, and because this is just the temperature where monolayer hydrazine desorbs from clean Al₂O₃, we attribute the shoulder to desorption of hydrazine from the first monolayer. Furthermore, comparison of the intensity of this shoulder with the corresponding peak for Al₂O₃ suggests that ca. 30–60% of the hydrazine present in the first monolayer on Ir/Al₂O₃ desorbs intact. This fraction is close to the 50% ML equivalent Ir coverage, and the fact that the desorption temperature is identical to that for clean Al₂O₃ suggests that the Ir-free areas of the sample account for most desorption of the intact first monolayer of hydrazine. If this analysis is correct, then hydrazine bound to Ir primarily decomposes rather than desorbing intact.

N_2 desorption peaks are observed at 215 and 570 K. Sawin et al.⁷ studied angle-resolved TPD of N_2 from hydrazine/Ir(111). They reported two N_2 desorption peaks at 290 and 500 K, and strong desorption angular dependence was observed only for the lower temperature peak. In a study of hydrazine decomposition on polycrystalline rhodium, Prasad et al.⁸ also observed two N_2 desorption peaks at 220 and 635 K.

As Figure 2 shows, ammonia desorption is observed in a sharp peak at 215 K and in a broad feature extending from ~ 290 to ~ 450 K. The 215 K feature has a peak temperature identical with and a width similar to those of the analogous low-temperature N_2 desorption feature, suggesting that the mechanisms leading to these desorption peaks are coupled. In contrast, the high-temperature NH_3 feature appears well below the high-temperature N_2 feature. Similar ammonia production behavior is seen on bulk metal surfaces. Sawin et al. did not show data for NH_3 in their hydrazine/Ir(111) TPD study, but they noted that NH_3 was seen in the same temperature regime as their low-temperature N_2 feature, but without the sharp angular dependence. Prasad et al.⁸ also observed two ammonia desorption features for hydrazine/rhodium, and again, the low-temperature NH_3 peak was coincident ($T_{\text{peak}} \approx 220$ K) with their low-temperature N_2 desorption peak. Also similar to what we see, they see a broad NH_3 desorption feature at higher temperatures, although, for Rh, this feature appears as a tail on the sharp low-temperature peak, rather than as a distinct peak. The desorption features we observe for hydrazine/Ir/ Al_2O_3 are at somewhat different temperatures than in the two single crystal studies, but the general similarities suggest that the decomposition mechanisms are not drastically different.

The other major product shown in Figure 2 is hydrogen. Here we show both the raw spectrum and the spectrum corrected for ionizer fragmentation of hydrazine. For H_2 , there is the additional complication of ionizer fragmentation of NH_3 to mass 2; however, the NH_3 intensity is too low (note scale factors in Figure 2a) for the $\text{NH}_3 \rightarrow \text{H}_2^+$ contribution to be significant. In any case, by comparison of the TPD spectra for masses 2, 17, and 32, it is possible to work out the H_2 desorption behavior. In the raw spectrum there is a sharp mass 2 peak at 164 K, resulting from ionizer fragmentation of desorbing multilayer hydrazine. After correction of the spectrum by subtraction of the scaled hydrazine spectrum, two mass 2 components remain. The broad peak appearing at ~ 320 K, and extending to ~ 500 K, appears neither in the mass 32 nor mass 17 spectrum. This peak, therefore, is unambiguously attributable to desorption of H_2 decomposition products, presumably generated by recombination of H_{ads} .

The corrected mass 2 spectrum also has substantial intensity in the 180–300 K range; however, it is not clear how much of this signal represents actual H_2 desorption. The absence of a sharp peak at 215 K indicates that the contribution from NH_3 ionizer fragmentation is insignificant, as expected, but there is another, less quantifiable source of the background signal. Examination of the raw mass 2 spectrum shows that most of the “corrected” mass 2 intensity in the 180–300 K range originates in a tail extending to high temperatures from the multilayer peak at 164 K. Some fraction of this tail may simply be time-dependent background originating from hydrazine desorbing at 164 K, sticking on surfaces in the mass spectrometer, and then slowly desorbing. A tail is also observed in the hydrazine (mass 32) spectrum, but with much lower intensity relative to the peak, as might be expected if most hydrazine sticking on the hot mass spectrometer surfaces decomposes. If

this analysis is correct, then the apparent H_2 signal in the 180–300 K range is partly or entirely an artifact.

On the other hand, the literature suggests that a real H_2 desorption feature in the 180–300 K range is not unlikely. Unfortunately, high mass 2 background prevented Sawin et al.⁷ from monitoring H_2 in their TPD study of hydrazine/Ir(111). Prasad et al.⁸ did monitor H_2 in their TPD study of hydrazine/Rh foil, and because their results for NH_3 and N_2 are qualitatively similar to what we observe for hydrazine/Ir/ Al_2O_3 , the comparison is interesting for H_2 . For hydrazine coverage in our range, two H_2 peaks are observed at ~ 300 and ~ 460 K, suggesting that a bimodal desorption spectrum is not unreasonable. H_2 TDP from $\text{H}_2/\text{Ir}(110)-(1 \times 2)$ was also found to be bimodal by Ibbotson et al.²³ One peak, at 400 K, is in the same temperature range as the broad high-temperature H_2 peak we observe. The other peak drops from ~ 300 to ~ 200 K with increasing hydrogen coverage. Both features were shown to result from recombinative desorption, and were attributed to H_{ads} bound at different sites on the highly corrugated Ir(110)-(1 \times 2) surface. Nieuwenhuys et al. studied H_2 desorption from Ir(111); however, the lowest adsorption temperature studied was 273 K; thus, their results do not address the low-temperature desorption behavior. $\text{H}_2/\text{Ir}(111)$ was, however, studied by Engstrom and Weinberg²⁴ in the temperature range of interest. They also only saw a single component peaking around 375 K. On the other hand, given the appearance of a second, lower temperature feature for the more open (110)-(1 \times 2) surface, it would not be surprising if supported Ir also has a low-temperature feature. We conclude that H_2 definitely desorbs in the broad feature from ~ 320 to 500 K, and that there may be a second H_2 desorption feature at lower temperature.

One issue is whether the desorption features are controlled by N_2 and NH_3 desorption kinetics, or by the kinetics of hydrazine decomposition. Several observations suggest that the low-temperature desorption features are controlled by hydrazine decomposition. A key observation is that the N_2 and NH_3 low-temperature features have nearly identical temperature dependencies in both our experiments and in the bulk metal surface work of Prasad et al.⁸ and Sawin et al.⁷ If detection of either product were limited by desorption kinetics, then identical temperature dependencies would be unlikely. Furthermore, Sawin et al. found that the low-temperature N_2 feature had sharp angular dependence, and concluded that the low-temperature N_2 feature results from direct reaction on the surface, generating N_2 that experiences strong repulsion as it desorbs.

N_2 and NH_3 TPD experiments on various Ir surfaces provide another valuable point of comparison. Cornish et al.²⁵ measured N_2 TPD from Ir(111), and found several N_2 desorption features, all below ~ 200 K, corresponding to desorption of molecularly adsorbed N_2 . In contrast, N_2 produced by recombination after NO dissociative adsorption was found to desorb at temperatures between ~ 350 and 500 K. EELS measurements indicated no N_2 bound on the surface in this temperature range; i.e., N_2 produced by recombination desorbs immediately as expected from the low desorption temperatures measured for molecularly adsorbed N_2 . Carabineiro et al.²⁶ measured TPD after adsorbing NH_3 at 300 K on the highly corrugated Ir(110) surface. NH_3 desorption was observed at ~ 400 K, with N_2 desorption at ~ 640 K. Santra et al.²⁷ examined ND_3 TPD after adsorption at 100 K on Ir(100). ND_3 desorption was observed in the 300–400 K range for monolayer or submonolayer coverages, with multilayer desorption appearing below 200 K. D_2 desorption was reported at 470 K, and N_2 desorption at 510 K. Coadsorption of H_2 and ND_3 leads to some HD desorption, and a stepwise ND_3

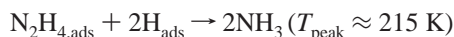
decomposition mechanism was proposed. The photoemission study of Purtell et al.²⁸ for NH₃ adsorbed on Ir(111) at 230 K provides an interesting contrast. At this temperature, ammonia appears to bind molecularly to the close-packed surface. In summary, the NH₃, H₂, and N₂ desorption temperatures measured on the more open Ir(100) and Ir(110) surfaces are all in the same range as those of the high-temperature features we observe for hydrazine products (NH₃, 280–450 K; H₂, 320–500 K; N₂, 500–650 K), but well above that (215 K) of the sharp features observed for N₂ and NH₃. Finally, we also looked for N₂ thermal desorption following ammonia dosing of our Ir/Al₂O₃ sample at room temperature, i.e., above the temperature where the low-temperature ammonia product desorbs. A broad N₂ peak is observed in the temperature range from ~500 to 650 K—nearly identical to that of the high-temperature N₂ feature we observe in hydrazine decomposition.

On the basis of our results and the related studies discussed above, the hydrazine decomposition mechanism seems to break down into distinct low- and high-temperature parts.^{4,5,8} As suggested by Sawin et al.,⁷ the sharp low-temperature N₂ peak is attributed to a direct decomposition reaction on the surface, generating N₂ that desorbs without associating with the surface:



The nearly identical desorption feature for NH₃ at low temperatures suggests that the N₂ and NH₃ production mechanisms are coupled. Our NH₃/Ir/Al₂O₃ TPD results suggest that NH₃ dissociatively adsorbs on the catalyst, at least above 300 K, and other TPD studies of NH₃ on various Ir surfaces also see NH₃ desorption only at temperatures well above 215 K. Therefore, we conclude that the NH₃ is produced in such a way that at least some fraction does not become bound to Ir, and desorbs promptly.

Several NH₃ production mechanisms are possible, depending on how hydrazine is bound on Ir/Al₂O₃ at low temperature. Unfortunately, we have not found any low-temperature spectroscopy for hydrazine on Ir/Al₂O₃ providing information on the binding motif. If substantial N₂H_{4,ads} is present, then NH₃ might be generated in reaction with H_{ads} from the N₂ generation reaction:



Alternatively, if N₂H₄ is dissociatively adsorbed at low temperatures, then NH₃ could be generated by reaction with surface radical species, such as NH₂:



In either case, the reaction could occur by H diffusion from neighboring sites on the Ir surface, but also could occur via a concerted mechanism in a complex, as has been suggested by some authors.^{7,29} If H₂ also desorbs at low temperature (see above), it would presumably have to form by recombination of H_{ads}. Even if some low-temperature H₂ desorption occurs, it is clear that a substantial fraction of the hydrogen remains on the surface to desorb as H₂ and NH₃ at high temperatures.

In addition to the low-temperature mechanism, all three products are also observed to desorb in broad, overlapping features in the temperature range from ~280 to 650 K. On the basis of the similarities of these desorption features to those observed following dissociative adsorption of NH₃ on various Ir surfaces,^{26,27} the high-temperature features are attributed to recombination of N_xH_y species left on the surface by hydrazine

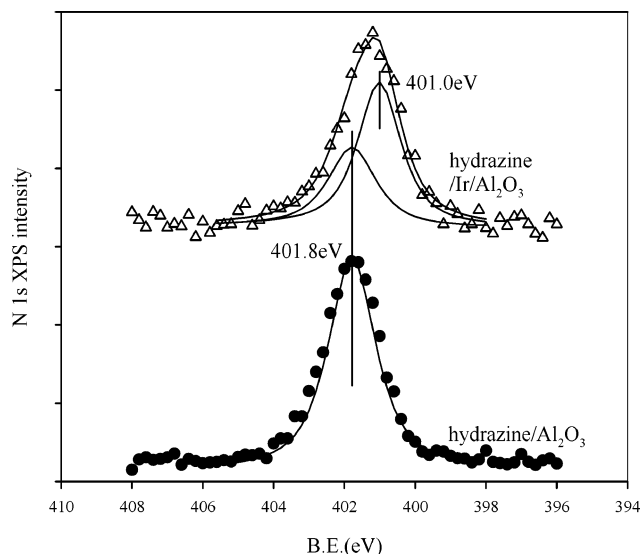
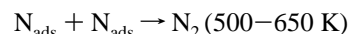
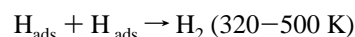
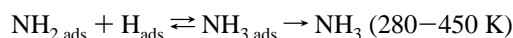
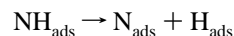


Figure 3. Nitrogen 1s XPS following hydrazine dosing of clean Al₂O₃/NiAl(110) (bottom spectrum) and of a sample with 0.5 ML equivalent of Ir⁺ deposited onto Al₂O₃/NiAl(110) (top spectrum). The symbols show the raw data, and the solid lines are fits.

decomposition. Such a mechanism can be written in different ways, but a reasonable set of reactions is^{4,5,8}



Consistent with this sequential mechanism is the observation that, once the temperature is high enough to drive recombinative desorption of H₂, the associated reduction in H_{ads} concentration rapidly shuts down NH₃ production.

B. XPS Probing of TPD Effects on the Sample State. Figure 3 shows N 1s XPS spectra of Al₂O₃ and Ir/Al₂O₃ samples following a 2.7 langmuir hydrazine dose at 93 K. For hydrazine/Al₂O₃ under these conditions, the TPD results show that there should be both first-monolayer and multilayer hydrazine present, but no decomposition products. The spectrum is well fit with a single peak at 401.8 eV, indicating that the binding energy shift between monolayer and multilayer hydrazine is insignificant, consistent with the low desorption temperatures seen for both in TPD. For the hydrazine/Ir/Al₂O₃ sample, TPD indicates that there are significant binding differences for first-monolayer hydrazine bound to iridium vs Al₂O₃. The corresponding N 1s XPS peak is clearly shifted to lower binding energy and broadened, relative to the XPS peak for hydrazine/Al₂O₃. The spectrum can fit well by two peaks. One, at 401.8 eV, is unshifted from the value for hydrazine/Al₂O₃, and therefore is assigned to weakly bound, intact hydrazine, in both the multilayer and bound to clean Al₂O₃ regions. The second peak is shifted to 401.0 eV, and represents either hydrazine decomposition products or hydrazine bound strongly to Ir particles. We note that, in a study of hydrazine adsorption on metal surfaces, strong metal–nitrogen bonding was found to give low XPS binding energies, while higher XPS binding energies were

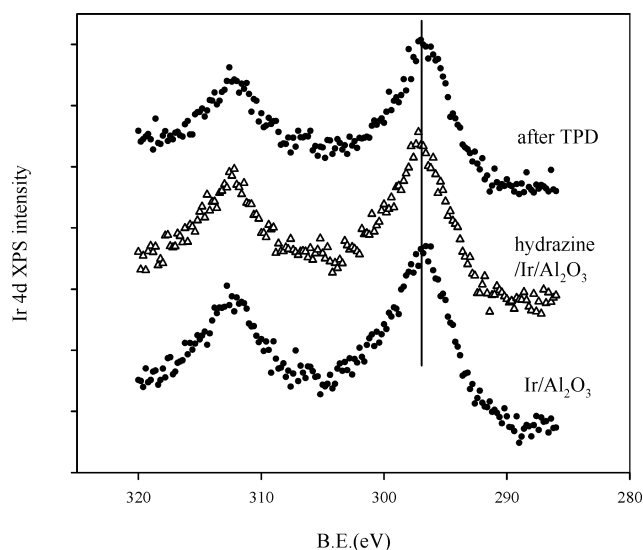


Figure 4. Ir 4d XPS of as-deposited Ir/Al₂O₃/NiAl(110) (bottom), after 2.7 langmuir hydrazine exposure (middle), and after a TPD run (top).

found for cases with metal–nitrogen bonding that was either weak or nondirect (i.e., the free NH₂ in a linear metal–NH=NH₂ geometry).³

In contrast to the binding energy shifts observed for N 1s XPS, Figure 4 shows that the Ir 4d binding energy is identical for as-deposited Ir/Al₂O₃ and hydrazine/Ir/Al₂O₃. As expected, adsorption of 2.7 langmuirs of hydrazine does result in ~18% attenuation of the Ir 4d signal because of electron scattering in the adsorbed layer. Similarly, ~17% attenuation is also observed for the Al 2p XPS signal from the substrate. Figure 4 also shows that the Ir 4d signal after a TPD experiment is attenuated by ~30% relative to that for the as-deposited sample, even though the hydrazine overlayer has desorbed. This attenuation most likely results from sintering of the Ir into larger particles. Ir evaporation or diffusion into the bulk would also account for the attenuation; however, we note that preparation of high-surface-area Ir/Al₂O₃ catalysts involves heating to temperatures near 800 K for much longer times than in our TPD experiments, suggesting that substantial evaporation or diffusion to the bulk is unlikely. If sintering is solely responsible for the XPS attenuation, and we assume that the as-deposited sample has all Ir on the surface, then 30% attenuation would require formation of particles with an average thickness of 4.7 layers. Given that our Ir dose is only 0.5 ML equivalent, the attenuation suggests that most of the Ir collects into large particles on the Al₂O₃ surface.

Figure 5 shows the N XPS spectra after a hydrazine TPD run for clean Al₂O₃ and for Ir/Al₂O₃. For hydrazine on clean Al₂O₃, no signal remains after TPD, indicating that no N-containing species are left on the surface. This result is expected from the TPD data, where only intact hydrazine was observed desorbing from clean Al₂O₃. In contrast, the Ir/Al₂O₃ sample has a significant residual N 1s peak, shifted substantially to low binding energy (~398 eV), compared to the two N 1s peaks observed prior to TPD (401.1 and 401.8 eV). Such a low binding energy is characteristic of nitrogen in strongly bound compounds such as metal nitrides or cyanides.³⁰ Because carbon levels in our system are negligible, cyanides are not possible, and we infer formation of a nitride or nitride-like compound. From comparison of the N 1s intensity in Figure 5 with the intensity prior to TPD (Figure 3, top), we can estimate the hydrazine-to-nitride conversion efficiency for a single TPD run. Because TPD shows that the multilayer hydrazine desorbs intact, we

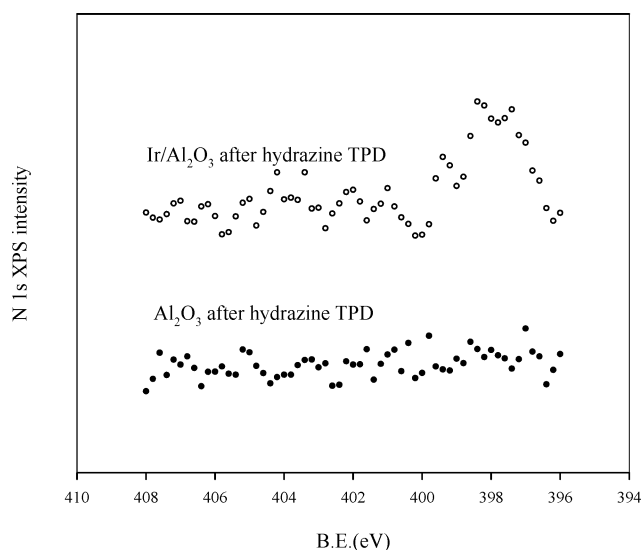


Figure 5. N 1s XPS spectra after TPD: bottom, Al₂O₃; top, Ir/Al₂O₃.

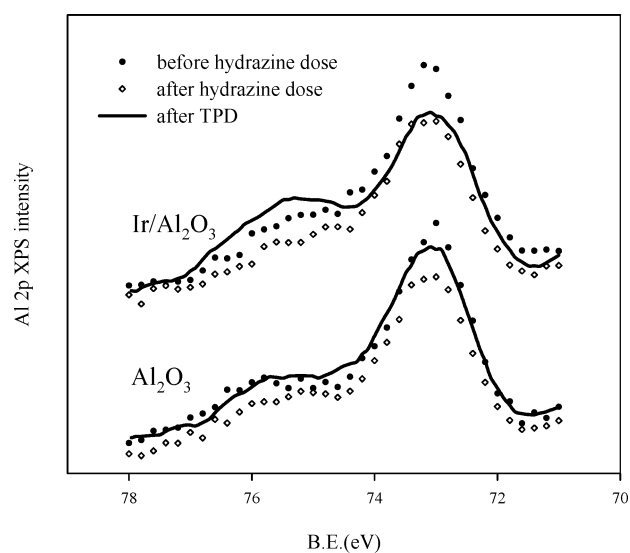


Figure 6. Al 2p XPS spectra of clean Al₂O₃/NiAl(110) and Ir/Al₂O₃/NiAl(110): solid symbols, as prepared, prior to hydrazine exposure; open symbols, after 2.7 langmuir hydrazine exposure; solid line, after TPD.

compare the post-TPD intensity with that of only the 401.1 eV component of the pre-TPD spectrum. The estimated hydrazine-to-nitride conversion efficiency for a single TPD run is 13%—surprisingly high.

The Ir XPS spectra in Figure 4 show no sign of the shift in Ir binding energy that would be expected if an iridium nitride were forming. Figure 6 shows, however, that there are significant changes in the Al 2p XPS. In those spectra, the peak at ~73 eV binding energy is from metallic aluminum in the NiAl bulk, a binding energy near that of pure Al metal.³⁰ The shoulder at ~75 eV in the “before hydrazine dose” spectra is from Al³⁺ in the Al₂O₃ oxide film. Upon hydrazine dosing, the entire spectrum is attenuated by the hydrazine overlayer, but there is no significant change in the ratio of metallic Al to Al³⁺. After TPD, the spectrum of the pure Al₂O₃ sample is nearly identical to that taken before hydrazine exposure, indicating that the oxide layer composition and thickness are essentially unaffected by hydrazine TPD. In contrast, the Ir/Al₂O₃ sample shows a substantial post-TPD increase in the 75 eV shoulder, indicating the presence of additional oxidized Al. Because TPD introduces no oxygen to the system, we infer that this aluminum is involved

in the nitride-like compound revealed by the N 1s XPS. Comparison of the pre- and post-TPD Al XPS shows that there is net conversion of metallic Al to oxidized Al; i.e., the nitride adds to, rather than replaces, the oxide film. Also consistent with this point is the observation that TPD results in no changes in the O 1s XPS; i.e., no oxygen is lost from the thin Al₂O₃ film as the nitride forms. The stoichiometry and formation mechanism of the Al_xO_yN_z product are unclear. Evidently, N_{abs} formed on the Ir particles can migrate and react with the underlying Al₂O₃ film at the high temperatures reached prior to N₂ recombinative desorption.

C. Hydrazine Decomposition on Size-Selected Clusters at Constant Temperature. Four samples were prepared by deposition of mass-selected Ir_n⁺ (*n* = 1, 5, 7, 10) at an energy of 1 eV/atom. For these studies, we wanted to use a lower Ir density to minimize cluster–cluster interactions and sintering. For Ir₅, Ir₇, and Ir₁₀, the density was 8.0×10^{13} atoms/cm², equivalent to 5% of that of a close-packed Ir monolayer. Because activity was found to be substantially lower for Ir₁/Al₂O₃, a density of 1.6×10^{14} atoms/cm² (10% ML equivalent) was used—still just 20% of the density used in the studies above. In the results shown below, the sample reactivity has been scaled for this difference in Ir density. In studies of Ir_n⁺, Au_n⁺, and Ni_n⁺ deposition on TiO₂, we found a 1 eV/atom deposition energy to be low enough that the clusters deposited more or less intact, i.e., without much fragmentation or sintering at room temperature.^{16,17,31} Of course, sintering or fragmentation on Al₂O₃ may be more important. Additional studies of the cluster impact energy dependence of sample morphology are planned, and here we confine ourselves to noting that the results below indicate that at least some memory of the deposited size remains.

The observation by XPS (above) that TPD causes major changes to the sample, probably by sintering, prompted use of a different probe of catalytic activity for the size-selected samples. The method relies on the fact that we deposit Ir in a ~ 2 mm diameter spot on a 7×7 mm Al₂O₃/NiAl substrate, and that our differentially pumped mass spectrometer views the sample through an aperture matched to the cluster spot size. It is possible, therefore, to monitor desorption from the Ir-containing spot, or from clean Al₂O₃, simply by translating the sample. After Ir_n⁺ deposition, each sample was exposed to a steady-state hydrazine pressure of 5×10^{-8} Torr at 300 K. This temperature is above the desorption temperature of hydrazine on clean Al₂O₃ and above the low-temperature desorption features on Ir/Al₂O₃. The NH₃ product signal was monitored continuously for 60 min, during which time the sample was translated so that the mass spectrometer alternately viewed regions of the surface with and without Ir_n. The difference in NH₃ signal between the two viewing areas was taken as a measure of activity. The temperature was then ramped (1 K/s) to 400 K, and the experiment repeated. The 300 and 400 K results are shown in Figure 7, which compares the reactivities of the four different cluster sizes. The results are given as relative NH₃ signal *per* deposited Ir atom. The uncertainty is estimated to be $\sim 15\%$ in comparing the different cluster sizes and temperatures. At a sample temperature of 300 K, we find a substantial increase in NH₃ production when going from the sample prepared with Ir⁺ deposition to the samples prepared with preformed clusters. In addition, there is a weak trend to higher activity as the deposited cluster size increases from Ir₅⁺ to Ir₁₀⁺, although the individual differences are within our estimated uncertainty. This size dependence suggests several things. First, it clearly indicates that the sample properties are influenced by the deposited cluster size, i.e., that sintering or

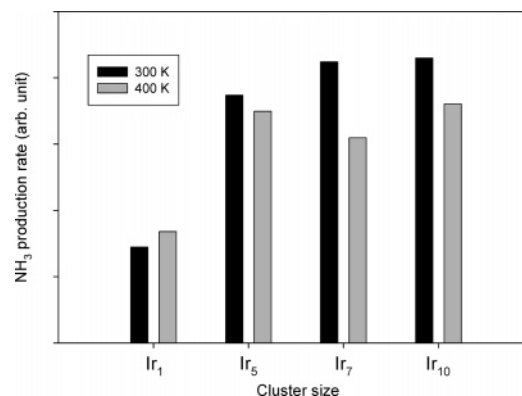


Figure 7. Relative NH₃ production per deposited Ir atom as a function of cluster size and for 300 and 400 K surface temperatures.

fragmentation of the clusters at room temperature under hydrazine flux does not erase memory of the initial cluster size. The significantly higher activity for Ir_n⁺ (*n* ≥ 5) compared to Ir⁺ suggests, therefore, that hydrazine decomposition activity depends strongly on cluster size, at least for very small clusters.

At 400 K, there are no changes in activity outside of our uncertainty; however, it appears that the activity of the samples prepared with clusters decreases relative to that for the Ir⁺-prepared sample. This change is what might be expected if thermally induced or adsorbate-induced sample modifications are erasing the dependence on the deposited cluster size. Data were taken at higher temperatures as well, and the general trend appears to continue. Unfortunately, we consider these data too uncertain for publication. The problem is that the continuous relatively high hydrazine pressure resulted in rising background at all decomposition product masses, presumably from various hydrazine decomposition chamber, sample mount, and mass spectrometer surfaces. The higher temperature data are more uncertain because they were taken later in the experimental sequence. Rather than attempting to refine this continuous exposure approach, we will construct an all-Teflon-and-glass pulsed inlet system, allowing us to study higher peak hydrazine pressures, but with a much lower average background pressure.^{31,32}

IV. Conclusions

Hydrazine decomposition was studied by TPD on model catalysts prepared by deposition of 0.5 ML equivalent of Ir⁺ on Al₂O₃/NiAl. These are the first TPD studies of hydrazine/Ir/Al₂O₃ decomposition at cryogenic temperatures, and the results are qualitatively in agreement with hydrazine TPD experiments on single-crystal Ir and polycrystalline Rh. Hydrazine decomposition at ~ 215 K is observed, leading to prompt desorption of N₂, NH₃, and possibly H₂. Species left on the surface undergo further reactions at increasing surface temperatures, generating NH₃, H₂, and finally N₂.

XPS was used to probe hydrazine TPD-induced changes in the samples. A substantial decrease in the Ir XPS intensity suggests that considerable sintering takes place when the samples are heated to 800 K. In addition, $\sim 13\%$ of the nitrogen is left on the surface, and from the binding energy shifts, it appears that an aluminum nitride (or mixed Al_xO_yN_z) compound is forming, catalyzed by the presence of Ir.

Continuous flow experiments were used to probe relative reactivity at 300 and 400 K of samples prepared by depositing differently sized Ir_n⁺ clusters. At 300 K, samples prepared with preformed Ir_n⁺ (*n* = 5, 7, 10) are about twice as active, per Ir atom, as samples prepared with Ir⁺ deposition, and there is a

weak increase with cluster size from $n = 5$ to $n = 10$. At 400 K the trends are similar, but weaker, suggesting that sintering is already significant.

Acknowledgment. This work was supported by the U.S. Air Force Office of Scientific Research, under Grant F49620-03-1-0062.

References and Notes

- (1) Ranney, J. T.; Gland, J. L. *Surf. Sci.* **1996**, *360*, 112.
- (2) Daniel, W. M.; White, J. M. *Surf. Sci.* **1986**, *171*, 289.
- (3) Alberas, D. J.; Kiss, J.; Liu, Z.-M.; White, J. M. *Surf. Sci.* **1992**, *278*, 51.
- (4) Dopheide, R.; Schröter, L.; Zacharias, H. *Surf. Sci.* **1991**, *257*, 86.
- (5) Rauscher, H.; Kostov, K. L.; Menzel, D. *Chem. Phys.* **1993**, *177*, 473.
- (6) Carabineiro, S. A. C.; Nieuwenhuys, B. E. *Surf. Sci.* **2003**, *532*–*535*, 87.
- (7) Sawin, H. H.; Merrill, R. P. *J. Chem. Phys.* **1980**, *73*, 996.
- (8) Prasad, J.; Gland, J. L. *Langmuir* **1991**, *7*, 722.
- (9) Falconer, J. L.; Wise, H. *J. Catal.* **1976**, *43*, 220.
- (10) Chen, X.; Zhang, T.; Xia, L.; Li, T.; Zheng, M.; Wu, Z.; Wang, X.; Wei, Z.; Xin, Q.; Li, C. *Catal. Lett.* **2002**, *79*, 21.
- (11) Choudhary, T. V.; Sivadinarayana, C.; Goodman, D. W. *Catal. Lett.* **2001**, *72*, 197.
- (12) Xiao, F.-S.; Weber, W. A.; Alexeev, O.; Gates, B. C. *Stud. Surf. Sci. Catal.* **1996**, *101*, 1135.
- (13) Zhao, A.; Gates, B. C. *J. Am. Chem. Soc.* **1996**, *118*, 2458.
- (14) Alexeev, O.; Panjabi, G.; Gates, B. C. *J. Catal.* **1998**, *173*, 196.
- (15) Boyd, K. J.; Lapicki, A.; Aizawa, M.; Anderson, S. L. *Rev. Sci. Instrum.* **1998**, *69*, 4106.
- (16) Aizawa, M.; Lee, S.; Anderson, S. L. *J. Chem. Phys.* **2002**, *117*, 5001.
- (17) Aizawa, M.; Lee, S.; Anderson, S. L. *Surf. Sci.* **2003**, *542*, 253.
- (18) Jaeger, R. M.; Kühlenbeck, H.; Freund, H.-J.; Wuttig, M.; Hoffmann, W.; Franchy, R.; Ibach, H. *Surf. Sci.* **1991**, *259*, 235.
- (19) Andersson, S.; Brühwiler, P. A.; Sandell, A.; Frank, M.; Libuda, J.; Giertz, A.; Brena, B.; Maxwell, A. J.; Bäumer, M.; Freund, H.-J.; MDRtensson, N. *Surf. Sci.* **1999**, *442*, L964.
- (20) Bäumer, M.; Freund, H.-J. *Prog. Surf. Sci.* **1999**, *61*, 127.
- (21) Stein, S. E., Director. IR and Mass Spectra. In *NIST Chemistry WebBook, NIST Standard Reference Database Number 69*; Mallard, W. G., Linstrom, P. J., Eds.; NIST Mass Spectrometry Data Center, National Institute of Standards and Technology: Gaithersburg, MD, 2000; <http://webbook.nist.gov>.
- (22) Chrysostomou, D.; Flowers, J.; Zaera, F. *Surf. Sci.* **1999**, *439*, 34.
- (23) Ibbotson, D. E.; Wittrig, T. S.; Weinberg, W. H. *J. Chem. Phys.* **1980**, *72*, 4885.
- (24) Engstrom, J. R.; Tsai, W.; Weinberg, W. H. *J. Chem. Phys.* **1987**, *87*, 3104.
- (25) Cornish, J. C. L.; Avery, N. R. *Surf. Sci.* **1990**, *235*, 209.
- (26) Carabineiro, S. A. C.; Nieuwenhuys, B. E. *Surf. Sci.* **2002**, *505*, 163.
- (27) Santra, A. K.; Min, B. K.; Yi, C. W.; Luo, K.; Choudhary, T. V.; Goodman, D. W. *J. Phys. Chem. B* **2002**, *106*, 340.
- (28) Purtell, R. J.; Merrill, R. P.; Seabury, C. W.; Rhodin, T. N. *Phys. Rev. Lett.* **1980**, *44*, 1279.
- (29) Wood, B. J.; Wise, H. *J. Catal.* **1975**, *39*, 471.
- (30) Moulder, J. F.; Stickle, W. F.; Sobol, P. E.; Bomben, K. D. In *Handbook of X-ray Photoelectron Spectroscopy*; Chastain, J., King, R. C. J., Eds.; Physical Electronics: Eden Prairie, MN, 1995.
- (31) Lee, S.; Fan, C.; Wu, T.; Anderson, S. L. *J. Am. Chem. Soc.* **2004**, *126*, 5682.
- (32) Judai, K.; Abbet, S.; Worz, A. S.; Rottgen, M. A.; Heiz, U. *Int. J. Mass Spectrom.* **2003**, *229*, 99.